Earth and Planetary Science Letters 485 (2018) 19–31

Contents lists available at ScienceDirect

Earth and Planetary Science Letters

www.elsevier.com/locate/epsl

Southeastward increase of the late Quaternary slip-rate of the Xianshuihe fault, eastern Tibet. Geodynamic and seismic hazard implications

Mingkun Bai [a], Marie-Luce Chevalier [a,*], Jiawei Pan [a], Anne Replumaz [b], Philippe Hervé Leloup [c], Marianne Métois [c], Haibing Li [a]

[a] Key Laboratory of Continental Dynamics, Institute of Geology, Chinese Academy of Geological Sciences, 26 Baiwanzhuang Rd, Beijing 100037, China
[b] ISTerre, Université Grenoble Alpes, F-38400 Grenoble, France
[c] Laboratoire de géologie de Lyon, Université de Lyon 1, ENS de Lyon, CNRS, UMR 5276 LGL-TPE, F-69622 Villeurbanne, France

ARTICLE INFO

Article history:
Received 19 September 2017
Received in revised form 24 December 2017
Accepted 28 December 2017
Available online xxxx
Editor: A. Yin

Keywords:
Xianshuihe fault system
Selaha fault
eastern Tibetan Plateau
late Quaternary slip rate
tectonic-geomorphology
earthquake hazard

ABSTRACT

The left-lateral strike-slip Xianshuihe fault system located in the eastern Tibetan Plateau is considered as one of the most tectonically active intra-continental fault system in China, along which more than 20 $M > 6.5$ and more than 10 $M > 7$ earthquakes occurred since 1700. Therefore, studying its activity, especially its slip rate at different time scales, is essential to evaluate the regional earthquake hazard. Here, we focus on the central segment of the Xianshuihe fault system, where the Xianshuihe fault near Kangding city splays into three branches: the Selaha, Yalahe and Zheduotang faults. In this paper we use precise dating together with precise field measurements of offsets to re-estimate the slip rate of the fault that was suggested without precise age constraints. We studied three sites where the active Selaha fault cuts and left-laterally offsets moraine crests and levees. We measured horizontal offsets of 96 ± 20 m at Tagong levees (TG), 240 ± 15 m at Selaha moraine (SLH) and 80 ± 5 m at Yangjiagou moraine (YJG). Using ^{10}Be cosmogenic dating, we determined abandonment ages at Tagong, Selaha and Yangjiagou of $12.5(+2.5/-2.2)$ ka, 22 ± 2 ka, and 18 ± 2 ka, respectively. By matching the emplacement age of the moraines or levees with their offsets, we obtain late Quaternary horizontal average slip-rates of $7.6(+2.3/-1.9)$ mm/yr at TG and $10.7(+1.3/-1.1)$ mm/yr at SLH, i.e., 5.7–12 mm/yr or between 9.6 and 9.9 mm/yr assuming that the slip rate should be constant between the nearby TG and SLH sites. At YJG, we obtain a lower slip rate of 4.4 ± 0.5 mm/yr, most likely because the parallel Zheduotang fault shares the slip rate at this longitude, therefore suggesting a ~5 mm/yr slip rate along the Zheduotang fault. The ~10 mm/yr late Quaternary rate along the Xianshuihe fault is higher than that along the Ganzi fault to the NW (6–8 mm/yr). This appears to be linked to the existence of the Longriba fault system that separates the Longmenshan and Bayan Har blocks north of the Xianshuihe fault system. A higher slip rate along the short (~60 km) and discontinuous Selaha fault compared to that along the long (~300 km) and linear Ganzi fault suggests a high hazard for a $M > 6$ earthquake in the Kangding area in the near future, which could devastate that densely populated city.

1. Introduction

Determining the slip-rates of major active faults is essential to understand continental tectonics and assess regional seismic hazard. However, such slip rate estimates often depend on the time scale at which they are measured. For example, slip rates deduced from GPS studies (geodetic time-scale: few years to few tens of years) are often lower than those deduced from the offset and dating of landforms (late Quaternary time scale: few tens of ka). This could either be due to slip rate variations through time, to technical shortcomings, or to the fact that the time necessary to capture a fault's average rate is longer than the geodetic time scale. Indeed, late Quaternary rates span multiple cycles while geodetic measurements spanning only a few years are potentially dependent on the seismic cycle. Also, long strike-slip faults do not necessarily have

* Corresponding author.
E-mail addresses: 1358575145fly@sina.com (M. Bai), mlchevalier@hotmail.com (M.-L. Chevalier), jiawei-pan@foxmail.com (J. Pan), anne.replumaz@univ-grenoble-alpes.fr (A. Replumaz), herve.leloup@univ-lyon1.fr (P.H. Leloup), marianne.metois@univ-lyon1.fr (M. Métois), lihaibing06@163.com (H. Li).

https://doi.org/10.1016/j.epsl.2017.12.045
0012-821X/

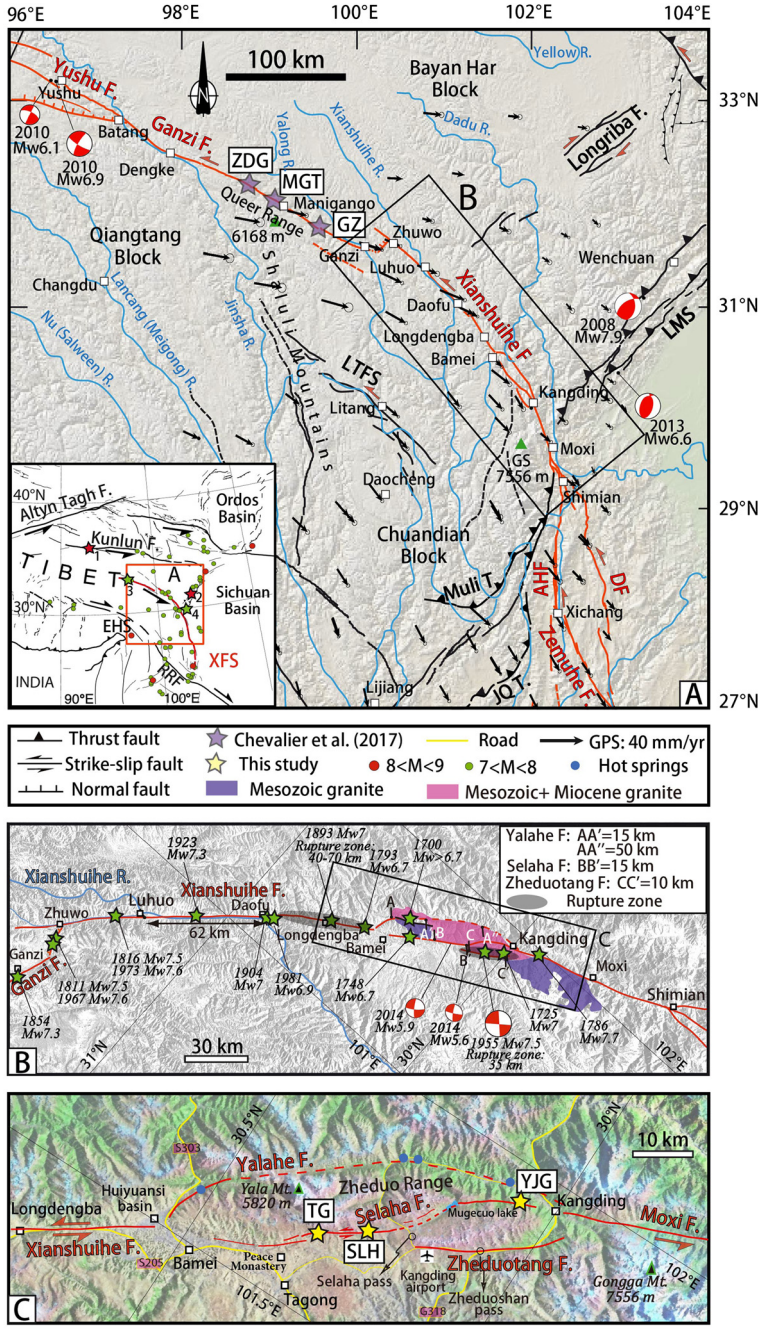

Fig. 1. The Xianshuihe fault system (XFS) in the frame of the India–Asia collision zone. (A) Tectonic map of eastern Tibet with digital elevation model (DEM) in the background. Horizontal GPS velocities relative to stable Eurasia (Liang et al., 2013), focal mechanisms of instrumental earthquakes with Mw > 5 (CMT catalog 1976–2016: 2008 Wenchuan, 2010 Yushu, 2013 Lushan and 2014 Kangding), as well as main peaks, cities, active faults (those of the XFS in red) and rivers. LMS = Longmenshan, AHF = Anninghe fault, DF = Daliangshan fault, LTFS = Litang fault system, JQT = Jinhe–Qinghe thrust, GS = Gongga Shan. Inset shows the Xianshuihe fault system within Asia, EHS = Eastern Himalayan syntaxis, RRF = Red River fault. Stars indicate location of major earthquakes: 1 = 2001 Ms8.1 Kokoxili earthquake, 2 = 2008 Ms8.0 Wenchuan earthquake, 3 = 2010 Mw6.9 Yushu earthquake, 4 = 2013 Ms7.0 Lushan earthquake. (B) Xianshuihe fault (box in A) with historical and recorded earthquakes (green stars with years and magnitudes), as well as rupture zones of the 1893 Bamei and the 1955 Kangding earthquakes (Wen et al., 2008). Gongga Shan batholith (purple and pink) offsets and Xianshuihe River offset are indicated. (C) Landsat satellite image of the SE Xianshuihe fault (box in B), where the main trace of the Xianshuihe fault splays into the Yalahe, Selaha and Zheduotang faults before reconnecting as the Moxi fault farther to the SE. Active faults are in red while inactive or less clear fault traces are dashed. (For interpretation of the references to color in this figure legend, the reader is referred to the web version of this article.)

a constant slip rate nor slip history along their full length. This reflects the geodynamic context that lead to their formation and evolution, and has strong implications on the seismic hazard. To assess these problems, we compare the slip rates for a particular segment of a major strike-slip fault at various time scales, and then compare it with the slip rates of another segment of the same fault zone: the Xianshuihe fault system in eastern Tibet.

The ~1400 km-long left-lateral strike-slip Xianshuihe fault system is one of the most tectonically active intra-continental fault system in China, separating the Bayan Har block from the Qiangtang block (e.g., Allen et al., 1991; Wen, 2000; Wen et al., 2008) (Fig. 1A). Almost its entire length has ruptured in nine Ms > 7 and sixteen Ms > 6 earthquakes since 1700 (Allen et al., 1991), with three earthquakes of Ms > 7.3 since 1923 along just the

Xianshuihe (hereafter XSH) fault segment (Allen et al., 1991; Wen, 2000) (Fig. 1B).

Despite the Xianshuihe fault system being a major tectonic feature in China, its late Quaternary slip rate has not been precisely determined yet, especially along the XSH fault segment. Late Quaternary horizontal slip rates between 8 and 20 mm/yr had been suggested for the XSH fault, using offset geomorphic features but with few quantitative age data (Allen et al., 1991), and with sometimes questionable offset determination and methodology (Chen et al., 2008; Zhang et al., 2016).

In this paper, we aim at constraining the late Quaternary horizontal slip rate of the SE XSH fault (Selaha segment) by dating offset moraines and levee crests of a debris flow, the Tagong (TG), Selaha (SLH) and Yangjiagou (YJG) sites. We then compare that slip rate with those proposed for the same segment at shorter (geodetic) and longer (geologic: 4–10 Ma) time scales and with the rates along the Ganzi fault farther to the NW along the same Xianshuihe fault system to discuss possible rate variations along strike. Finally we discuss the timing of initiation and slip rate history, as well as rates and geometry along the NW Xianshuihe fault system to better understand how deformation due to the India/Asia collision is accommodated in eastern Tibet and evaluate the seismic hazard.

2. Geological setting

The Xianshuihe fault system is divided into four main segments: the Yushu/Batang fault at the NW end, the Ganzi fault in the NW, the Xianshuihe fault (XSH) in the center and the Moxi–Anninghe–Zemuhe–Xiaojiang faults in the SE (Fig. 1A). The ~300 km-long XSH fault strikes N140°E along its NW section from Zhuwo to Bamei, where it is particularly linear and continuous, and offsets the course of the Xianshui River by 62 km (Fig. 1B) (e.g., Gaudemer et al., 1989; Yan and Lin, 2015; Zhang et al., 2017). The remarkable linearity of the XSH fault is interrupted by the Huiyuansi basin, after which the fault splays in three right-stepping en-echelon branches: the Yalahe fault to the north, the Selaha fault in the center, and the Zheduotang fault ~50 km farther to the SE (Fig. 1C). The former two faults merge near Kangding to become the Moxi fault. Such geometry suggests that the three faults could be connected at depth (e.g., Allen et al., 1991; Jiang et al., 2015a). Note that a complex 3D geometry may prevent earthquake ruptures to reach the surface, which may explain why the surface rupture of the 1955 M7.5 Kangding earthquake was limited to the length of the Zheduotang fault itself (27 km) (Jiang et al., 2015a) (Fig. 1B). The fault trace is very clear within the Huiyuansi basin (junction between the XSH and Yalahe/Selaha faults) with significant scarps of up to ~8 m fading out toward the SE end of the basin (Fig. S1). This broad and flat basin may have acted as a major segmentation break terminating the surface rupture associated to the 1893 M7 Longdengba (also called Bamei) earthquake (Allen et al., 1991; Shao et al., 2016) (Fig. 1B).

While there are several indications that the Selaha and Zheduotang faults are currently active with clear fault traces, offsets of geomorphic features, and earthquakes (1955 and 2014 Kangding earthquakes, Fig. 1B), the Yalahe fault lacks such evidence and while its trace is clear on the geological map, it is much less clear in the morphology, except for a few km at its NW extremity (Figs. 1C and S1A, H). This suggests that the Yalahe fault may have been inactive recently (Allen et al., 1991). Indeed, fast exhumation of the Zheduo Range, estimated using low temperature thermochronology, was only active between ~9 and ~4 Ma and dramatically decreased since then, interpreted as due to the jump of motion from the Yalahe fault, forming a restraining bend exhuming the Zheduo Range, to the Selaha fault, exhuming the Gongga Range to the south (Zhang et al., 2017) (Fig. 1C). Across the Yalahe fault, the part of the Gongga batholith that contains Miocene granite is left-laterally offset by 15 to 50 km (AA' and AA" in Fig. 1B).

The morphology of the active Selaha fault is the most clear between Bamei and the Selaha pass (Figs. 1C, S2 and S3B, F). There, numerous clear left-lateral and vertical offsets of levees and moraine crests, U-shaped valleys and gullies are visible, as well as numerous sag ponds, sometimes filled with lakes (Figs. 2, 3, and S2). Some fresh surface ruptures, possibly those of the 1893 Longdengba earthquake, can even be observed near the Peace Monastery (Fig. S2H, I). The fault trace becomes harder to follow a few kilometers NW of the Peace monastery and for a few kilometers SE of the Selaha pass (Fig. 1C). Farther to the SE, the fault trace becomes continuous and clear again near the Mugecuo Lake all the way to Kangding, to eventually become the Moxi fault (Fig. 1C). This 3 km-long lake has been interpreted as being a large sag pond along the fault due to the curved nature of the fault, i.e., representing a releasing bend (Allen et al., 1991). The Selaha fault appears to left-laterally offset the Miocene granite by ~15 km (BB' in Fig. 1B) (Roger et al., 1995).

SW of the Selaha pass, the Zheduotang fault runs along the Kangding airport, crosses the Zheduoshan pass, follows the valley going to Kangding but ends before reaching it (Figs. 1C, 4A and S3G). There, while its trace is clear in the topography with sag ponds and SW-facing scarps, finding offsets is more challenging partly due to the very steep slopes and rockslides (Fig. S3G). The Zheduotang fault appears to bound the Miocene granite to the south, but appears to offset the batholith by ~10 km (CC' in Fig. 1B). Adding up the offsets across both the Selaha and Zheduotang faults thus becomes 25 km (BB' + CC' in Fig. 1B).

3. Previously published slip rate estimates

Long-term studies have matched geological offsets of ~60 km (e.g., Wang et al., 1998; Wang and Burchfiel, 2000; Yan and Lin, 2015) with initiation ages of ~2–4 Ma (Wang et al., 1998), ~13 Ma (Roger et al., 1995), 5–13 Ma (Yan and Lin, 2015) and 17 ± 2 Ma (Wang et al., 2012), yielding a wide range of slip rates of ~3.5–30 mm/yr. Recently, Zhang et al. (2017) suggested, based on the exhumation age of the Zheduo Range, that the fault initiated at ~9 Ma, yielding a long-term horizontal slip rate of ~7 mm/yr since ~9 Ma.

At the late Quaternary time scale, Zhang (2013) proposed an average slip rate of 8–11 mm/yr along the main segment of the XSH fault, using upper terrace ages associated with the onset of terrace riser offsets, reinterpreting Chen et al. (2008)'s data who had obtained 17 ± 3 mm/yr using radiocarbon and Optically Stimulated Luminescence (OSL) dating, but using lower terrace ages instead. Indeed, because a riser may constantly be refreshed by the active river until the lower terrace is abandoned, taking the upper terrace age yields a maximum age for the offset and thus a minimum slip rate (e.g., Cowgill, 2007). Along the Ganzi fault, by applying their well-dated 19 ± 3 ka terrace age, obtained by ^{10}Be cosmogenic dating in a depth profile at the MGT site ~300 km farther to the NW (Fig. 1A), to the alluvial surfaces offset along the XSH fault, Chevalier et al. (2017) recently suggested a rate between 6.5 and 12 mm/yr.

Along the NW Yalahe fault, a late Quaternary horizontal slip rate has been suggested at 0.8 mm/yr, by inferring a ~13 ka age of a moraine offset by 10 m (Allen et al., 1991). Chen et al. (2016) suggested a ~1.5 mm/yr slip rate along the NW Yalahe fault by matching till ridges offset by <200–300 m with one thermoluminescence age of 168 ± 14 ka. While the NW part of the Yalahe fault bounding the Huiyuansi basin is clearly active (clear normal component consistent with a change of strike of the XSH fault, Fig. 1C), no earthquake occurred nor evidence of activity along its SE part has been found on aerial photographs (e.g., Allen et al., 1991).

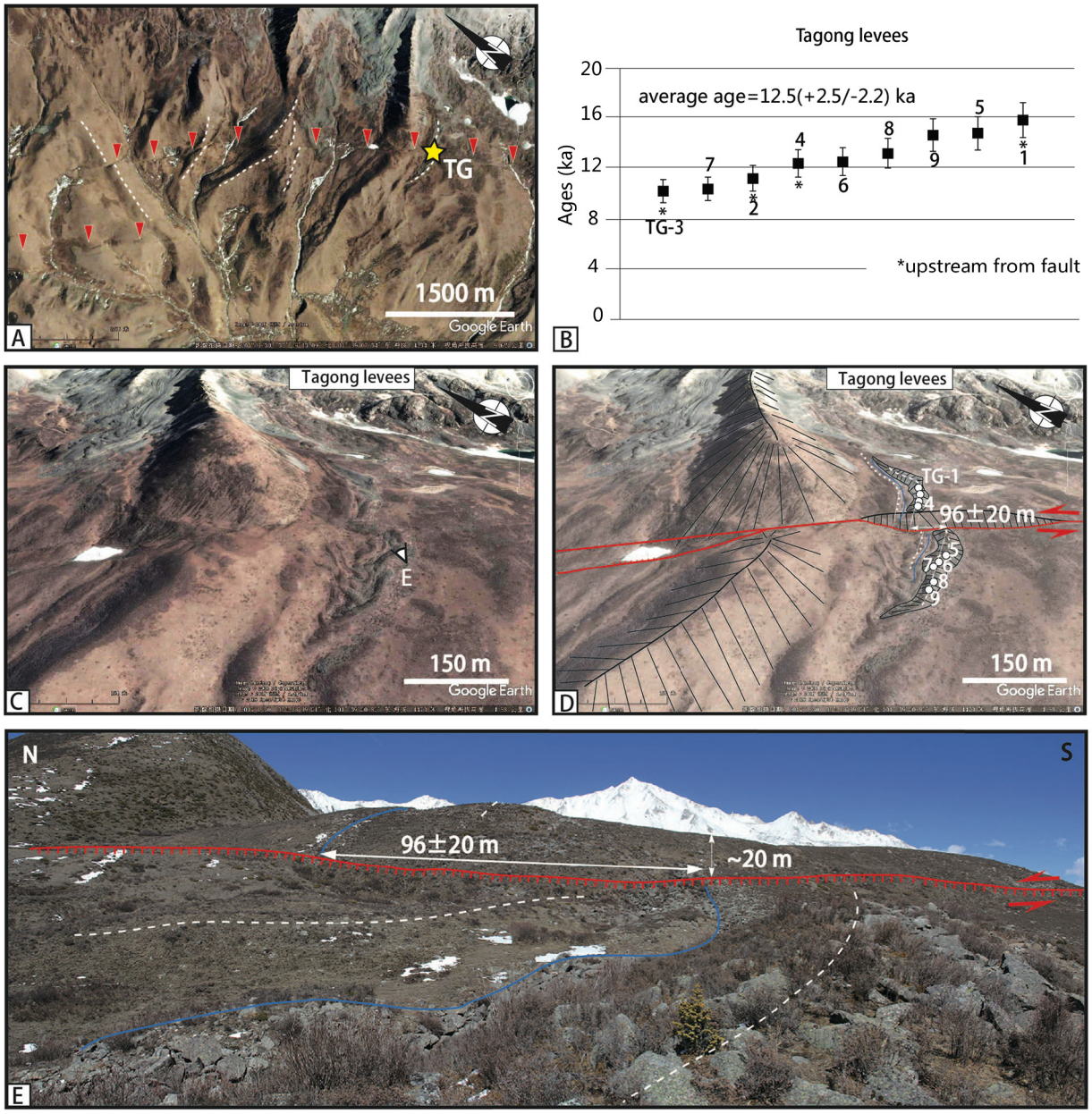

Fig. 2. Tagong (TG) site. (A) Google Earth image of the TG site area with the Selaha fault highlighted by the red triangles and the white dashed lines highlighting the offset geomorphic features (mostly moraine crests). (B) ^{10}Be cosmogenic surface-exposure ages of TG levees (using the Lal (1991)/Stone (2000) time-dependent model, bold in Table 1, "LS dep" column) with 1-sigma uncertainty. (C, D) Google Earth image of the TG levees (gray and chaotic surface) and its interpretation. Circles with numbers represent collected samples and white dashed lines highlight the levee crests. (E) Panoramic photo looking upstream at the TG site. The horizontal offset (96 ± 20 m) of the levee crests (in white) or of the small gully (in blue) in between is visible, as well as the ~20 m high scarp. (For interpretation of the references to color in this figure legend, the reader is referred to the web version of this article.)

Consequently, and following our own preliminary field observation along the central Yalahe fault, we thus suggest that the Yalahe fault is not active at present, even though Allen et al. (1991) suggested that the strike-slip component becomes predominant where the Yalahe fault becomes parallel to the XSH fault farther to the SE (Fig. 1C), which was most likely the case early on since the Yalahe fault has offset the batholith.

Slip rates along the Selaha fault have been inferred at 7.2 mm/yr in the central part (near the TG and SLH sites, Fig. 1C) and 4.6 mm/yr in the SE part (YJG site), by inferring an age of ~13 ka for moraines that are horizontally offset by 94 and 60 m, respectively (Allen et al., 1991). Similarly, Chen et al. (2016) suggested a qualitative rate of 6.7 ± 3 mm/yr by matching an inferred 18 ka age with an offset of 104 m (measured on satellite images) for the YJG moraine, and an inferred age of ~40 ka with an offset of 270 m (measured on satellite images) at the SLH site.

Few studies exist on the slip rate of the Zheduotang fault. Chen et al. (2016) suggested a late Quaternary horizontal rate of 8.5 ± 2 mm/yr from two sites. The first one consists of three gullies located near the Zheduoshan pass that are offset by ~142 m since 16.4 ka (OSL) while the second site is located at the SE terminus of the fault, where a presumably offset terrace riser (22 m) accrued in 2.3 ka (^{14}C, lower terrace age). However, we question the quality of these sites (no clear map nor exact location is given) and age assignment methodology (e.g., lower *vs* upper terrace reconstruction as explained above, and only one quantitative age). Similarly, Zhang et al. (2016) suggested a Holocene rate of ~6 mm/yr by matching a ~25 m horizontal offset of a gully with a ~4 ka radiocarbon age. We also question this latter study due to the lack of

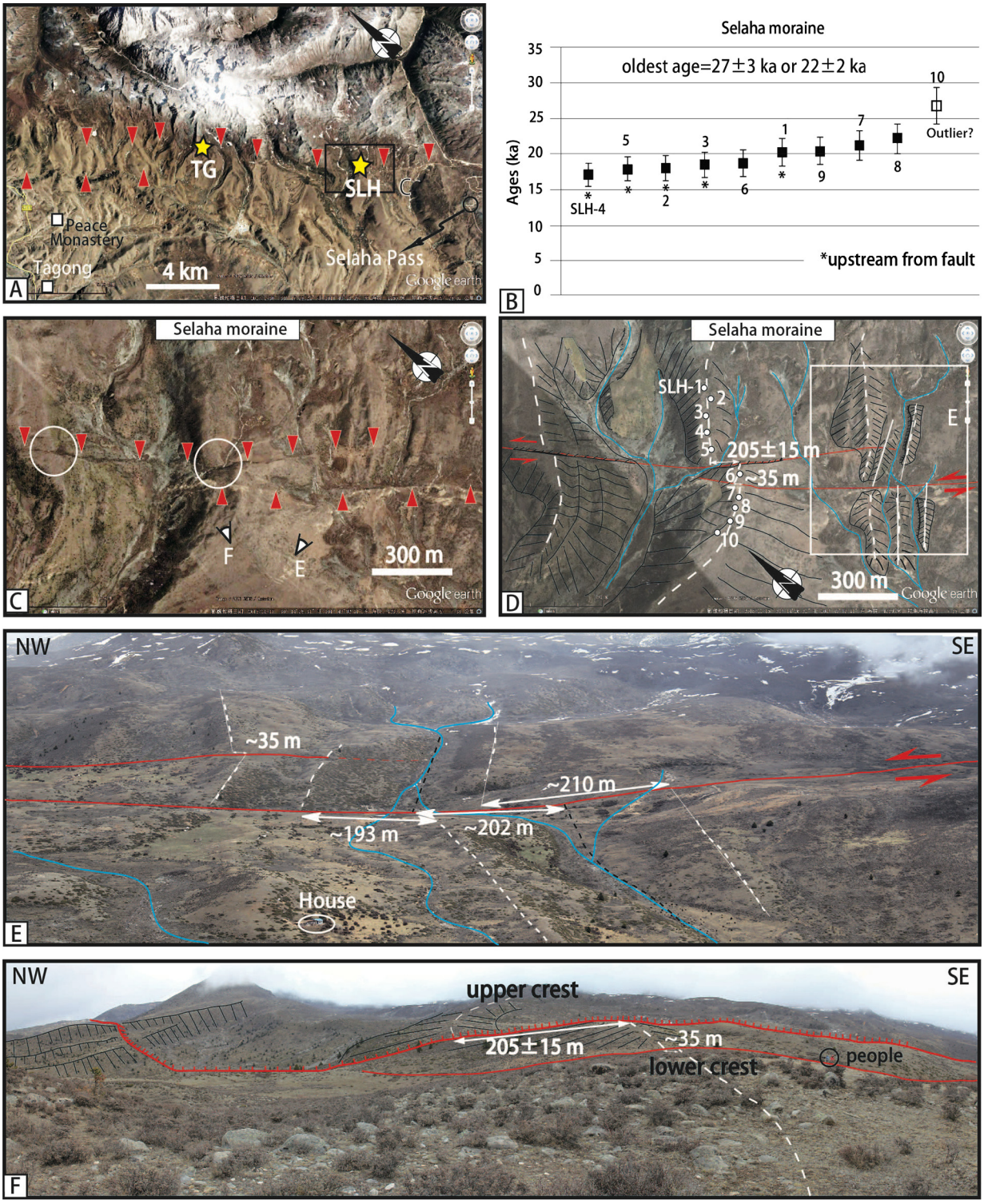

Fig. 3. SLH moraine (SLH) site. (A) Google Earth image of the Selaha fault (highlighted by red triangles) between the Peace monastery and the Selaha pass. (B) ^{10}Be cosmogenic surface-exposure ages of the SLH moraine (using the Lal (1991)/Stone (2000) time-dependent model, bold in Table 1, "LS dep" column) with 1-sigma uncertainty. (C, D) Close-up of the SLH moraine, with the two branches of the fault (upstream and downstream) showed by the red triangles, and its interpretation. White dashed lines represent the moraine crests, which are left-laterally offset by 205 ± 15 m along the upstream branch of the fault and by ~35 m along the downstream branch. (E) View of the offset gullies and ridges located just SE of the SLH moraine. The upstream branch offsets ridges by ~35 m while the downstream branch offsets several gullies and ridges by ~200 m. (F) Panoramic photo looking upstream at the SLH moraine. (G) Field photo of the NE-facing scarp just NW of the SLH moraine. (H) Field photo looking towards the SLH moraine, showing the scarp. (For interpretation of the references to color in this figure legend, the reader is referred to the web version of this article.)

exact location and site description (no figure nor photo provided). Therefore, we believe that the slip rate along the Zheduotang fault remains unconstrained.

On the geodetic time scale, InSAR data (1996–2008) suggest a rate of 9–12 mm/yr around Luhuo (Wang et al., 2009), and 7–7.4 mm/yr between Bamei and Kangding (Jiang et al., 2015b). The most recent GPS measurements across the XSH fault suggest strike-slip rates of 13–15 mm/yr (W. Wang et al., 2017), between 12.3 and 16.7 mm/yr (Y. Wang et al., 2017) and 8.0–10.2 mm/yr (Zheng et al., 2017), while older datasets sug-

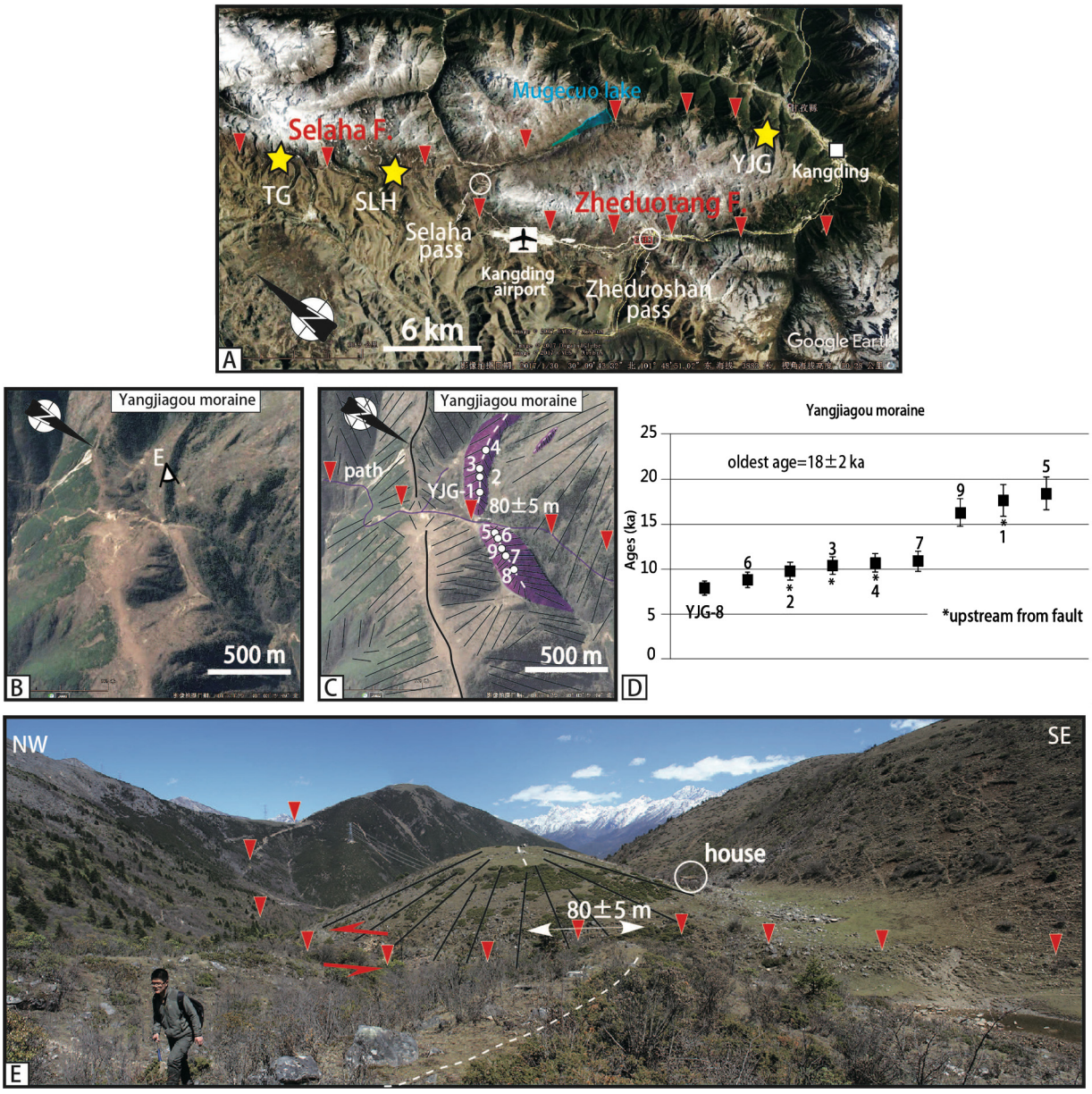

Fig. 4. SE Selaha fault and the Yangjiagou (YJG) site. (A) Google Earth image of the Selaha fault (highlighted by red triangles) between TG and Kangding. (B, C) Google Earth image of the Yangjiagou moraine and its interpretation. The 80 ± 5 m horizontal offset of the YJG crest is visible. (D) ^{10}Be cosmogenic surface-exposure ages of the YJG moraine (using the Lal (1991)/Stone (2000) time-dependent model, bold in Table 1, "LS dep" column) with 1-sigma uncertainty. (E) Panoramic photo looking downstream, with the Selaha fault highlighted by red triangles and the 80 ± 5 m offset. (For interpretation of the references to color in this figure legend, the reader is referred to the web version of this article.)

gest rates of 8–12 mm/yr (Shen et al., 2005), ~14.4 mm/yr (Gan et al., 2007), and 7.5–11.5 mm/yr (Zhang, 2013). This latter rate led Zhang (2013) to suggest a temporally constant slip rate along the XSH fault system of ~10 mm/yr since ~10 Ma.

4. Previous earthquake hazard considerations

The left-lateral strike-slip Xianshuihe fault system is the most seismically active intra-continental fault system in China, as almost its entire length has ruptured since 1700 by more than 20 M > 6.5 and 10 M > 7 earthquakes (Allen et al., 1991; Wen, 2000) (Fig. 1B). It has been observed that major recent earthquakes (Mw > 6.5) along the XSH fault migrated to the SE from Ganzi to Daofu (1967 Zhuwo, 1973 Luhuo and 1981 Daofu earthquakes, Fig. 1B), suggesting that the next big one may occur along the next segment to the SE, between Daofu and Bamei (e.g., Allen et al., 1991; Wen et al., 2008; Zhang et al., 2016). According to the coulomb stress theory, the earthquake hazard along the SE XSH fault has increased by a factor of two, equivalent to a decade of tectonic stress accumulation, able to produce a Mw > 7 earthquake, following the major 2008 Ms8.0 Wenchuan earthquake (e.g., Parsons et al., 2008; Toda et al., 2008; Yang et al., 2015) and the 2013 Ms7.0 Lushan earthquake (Shan et al., 2013; Yang et al., 2015). Indeed in 2014, two earthquakes (Kangding earthquakes: Mw5.9 event which triggered a Mw5.6 event, Figs. 1A, S4 and S5) occurred along the SE XSH fault, with slip mainly along the Selaha segment and to a lesser extent at the NW end of the Zheduotang segment. However, despite their significant magnitudes, these earthquakes did not entirely fill the Selaha seismic gap, i.e., the energy released was much less than that accumulated since the 1955 Kangding Mw7.5 event (Jiang et al., 2015a; Xie et al., 2017), which occurred on the same fault. Therefore, it still poses a seismic risk

for a Mw > 6–7 event (e.g., Allen et al., 1991; Jiang et al., 2015a; Shao et al., 2016), which suggests that the XSH fault may be late in its seismic cycle, with the 2014 Kangding earthquakes having acted as a minor seismic adjustment between the occurrence of larger earthquakes, following the 1955 Kangding earthquake (e.g., Yang et al., 2015).

5. Methods

The active Selaha fault perpendicularly cuts numerous moraines and alluvio-glacial geomorphic features, which is the optimal setting to study faulting behavior. We use a combination of field work and high-resolution satellite images to map active faults and offset geomorphic markers. We precisely measure their cumulative offsets using tape in the field, as well as by performing offset reconstruction from satellite images. The three study sites being quite remote, we could not conduct terrestrial LiDAR or kinematic GPS surveys.

We collected 28 samples from the top few centimeters of granite boulders (including three quartz veins at the TG site) that were present on the moraine or levee crests. The abandonment ages of the three sites were determined using ^{10}Be cosmogenic dating. The ^{10}Be concentration in surface boulders results mainly from nuclide accumulation due to exposure to cosmic rays at the sampling site. The oldest age on SLH and YJG moraine crests is chosen to best represent the moraine abandonment age because processes that yield apparent young ages (erosion, weathering, snow cover and rolling) are likely to have affected our samples (e.g., Putkonen and Swanson, 2003; Chevalier et al., 2011; Heyman et al., 2011). While prior-exposure (or inheritance) may affect our samples and yield apparent old ages, only <3% of boulders that were exposed prior to glacial erosion, transport and deposition, seem to be affected (Putkonen and Swanson, 2003; Heyman et al., 2011) because most of the inherited rocks have most likely been pulled off from the glacial valley, crushed, and eroded. These inherited samples (outliers) generally have ages that are much older than the rest of the population and can easily be discarded. In addition, a moraine surface may be relatively unstable after its emplacement, with large boulders being exhumed to the surface as erosion transports the finer material away therefore representing various stages of exhumation (e.g. Hallet and Putkonen, 1994; Putkonen and Swanson, 2003; Heyman et al., 2011). Consequently, the oldest age is the best choice to represent the moraine's abandonment age in the absence of clear outliers.

In contrast, the levees at TG are made of angular blocks and sparse soil in between because they have most likely been emplaced very rapidly, during an episode of massive melting (debris flow). Thus rolling and exhumation (through soil erosion) is less likely than on a moraine. Therefore the average age of the samples best represents the levees emplacement age.

By matching the abandonment age of the moraines or levees with their offsets, we obtain a late Quaternary median slip rate at the 1-sigma level (calculated using Zechar and Frankel, 2009).

6. Sites description and results

6.1. Tagong (TG) levees

The Tagong (TG) site is located ~13 km due east of the town of Tagong, at ~30.31°N–101.67°E at ~4500 m elevation (Figs. 1C and 2). A large rockslide fell from the adjacent steep slopes and high peaks of the Zheduo Range and later on a debris flow with parallel levees continued farther downstream, crossed the Selaha fault and was deposited until ~500 m downstream from the fault. Since their emplacement, the levees and the gully they separate have been left-laterally offset by 96 ± 20 m by the fault (Figs. 2D, E and S6). A vertical offset of 20 ± 5 m is also observed (west-facing scarp, Fig. 2E).

We collected nine samples from boulder tops located on the levee's southern crest, four upstream from the fault (TG-1-4) and five downstream (TG-5-9) (Figs. 2D, B and S5). The crests are mostly covered by angular boulders with small shrubs and grass in between (Fig. 2E). The sample ages are well-clustered and range from 10 ± 1 to 15 ± 1.5 ka and average at 12.5(+2.5/−2.2) ka (Fig. 2B and Table 1). Matching the horizontal offset with the TG levees emplacement age yields a late Quaternary horizontal slip rate of 7.6(+2.3/−1.9) mm/yr.

6.2. Selaha (SLH) moraine

The Selaha (SLH) moraines are located in the NW Zheduo Range, ~35 km NW of the city of Kangding or 9 km SE of the Tagong site (30.243°N, 101.716°E), at ~4240 m of elevation (Fig. 1C). The only present-day glaciers are located 15 km to the NW, near the Yala Mt. The SLH moraines we sampled are ~2.5 km-long and the crests are sub-rounded, with bushes, occasional trees, and medium-sized granite boulders (up to 2 m of diameter, Fig. S7).

Locally, the Selaha fault splits into two branches. The left-lateral offset of the SLH moraine crests is 205 ± 15 m (Figs. 3D, F and S8) along the upstream (north) branch of the fault and ~35 m along the downstream (south) branch, i.e., a total of 240 ± 15 m. From the SLH moraines, the upstream branch of the fault extends ~1.5 km to the east before its trace disappears, and it horizontally offsets a small ridge (moraine?) by ~35 m (Fig. 3E). The downstream branch then becomes the main fault and it left-laterally offsets gullies and ridges by ~193, ~202 and ~210 m, i.e., similar amounts as the SLH moraines (Fig. 3E). A 11 ± 2 m vertical offset of the SLH moraine is observed (east-facing scarp, Fig. S3C). These local scarps observed all along the Selaha fault are sometimes facing west (such as at TG) and sometimes facing east (such as here at SLH), most likely indicating that the Selaha fault is nearly vertical, as was suggested for the Ganzi fault farther to the NW, where the same scarp behavior is observed (Chevalier et al., 2017).

We collected ten samples from the top of the largest boulders that were present on the SLH moraine crests, five upstream (SLH-1-5) and five downstream (SLH-6-10) from the upstream fault (Figs. 3D and S7). The sample ages range from 17 ± 2 ka to 27 ± 3 ka, but with the oldest age being out of the 17–22 ka cluster of ages (Fig. 3B and Table 1). While matching the oldest age with the total offset (240 ± 15 m) yields a left-lateral slip rate of 9(+1.1/−0.9) mm/yr (SLH2 in Fig. 5), matching the next oldest age (22 ± 2 ka) with the same offset yields a slip rate of 10.7(+1.3/−1.1) mm/yr (SLH1 in Fig. 5). Indeed, the oldest age (SLH-10 – 26.8 ka) is older than the mean age of the population at the 2-sigma level (average age 19.4 ± 1.8 ka, MSWD = 1.7), strongly suggesting that it is an outlier. We favor the latter also because a last Glacial Maximum (LGM, ~20 ka) age at SLH is more in agreement with moraines dated elsewhere in eastern Tibet (e.g., Schafer et al., 2002; Strasky et al., 2009; Xu and Zhou, 2009; Xu et al., 2010; Zhang et al., 2012; Fu et al., 2013; Ou et al., 2014; Chevalier et al., 2017; this study at YJG, see below).

6.3. Yangjiagou (YJG) moraine

The Yangjiagou (YJG) moraines are located ~6 km NW of the city of Kangding or 30 km SE of the SLH site (30.052°N, 101.929°E), at ~3500 m of elevation (Fig. 1C). This part of the range does not have contemporary glaciers but numerous glacial lakes and very recent moraines abound towards the highest peaks, resembling a scoured terrain (Fig. 4A). However, few moraines are well-defined and present as low as 3500 m, which makes

Table 1
Analytical results of ^{10}Be geochronology and surface-exposure ages along the Xianshuihe fault system.

Sample name	Lat (°N)	Long (°E)	Elev (m)	Quartz (g)	Be carrier (mg)	^{10}Be/^{9}Be (10^{-15})	^{10}Be (10^{6} atom/g)	LS dep Ages (yrs)[a]
Tagong site								
Upstream from fault								
TG-1	30.309666	101.666921	4500	24.9605	0.242837	1343 ± 27	0.868 ± 0.018	**15461 ± 1476**
TG-2*	30.309633	101.666678	4498	22.521	0.231860	905 ± 24	0.617 ± 0.017	**11091 ± 1076**
TG-3	30.309596	101.666521	4499	23.2101	0.220369	893 ± 21	0.561 ± 0.013	**10091 ± 969**
TG-4*	30.309596	101.666521	4499	24.7262	0.235450	1078 ± 23	0.681 ± 0.015	**12240 ± 1170**
Downstream from fault								
TG-5*	30.308726	101.664946	4447	26.1026	0.236681	1314 ± 31	0.791 ± 0.019	**14510 ± 1395**
TG-6	30.308746	101.664744	4443	23.9193	0.230936	1045 ± 22	0.669 ± 0.014	**12364 ± 1181**
TG-7	30.308794	101.664587	4441	22.5454	0.264997	714 ± 18	0.555 ± 0.014	**10269 ± 990**
TG-8	30.308603	101.664046	4435	23.8159	0.247967	1017 ± 22	0.702 ± 0.015	**13024 ± 1246**
TG-9	30.308641	101.663477	4427	24.2903	0.252789	1122 ± 24	0.775 ± 0.017	**14373 ± 1375**
Selaha site								
Upstream from fault								
SLH-1	30.245064	101.717376	4271	22.1004	0.233091	1488 ± 30	1.043 ± 0.021	**20262 ± 1932**
SLH-2	30.244629	101.717552	4265	22.3408	0.230424	1332 ± 27	0.912 ± 0.019	**17977 ± 1723**
SLH-3	30.244172	101.716848	4242	24.5239	0.229808	1490 ± 48	0.928 ± 0.030	**18465 ± 1825**
SLH-4	30.243487	101.716246	4241	20.9960	0.220370	1218 ± 27	0.848 ± 0.019	**16997 ± 1636**
SLH-5	30.242491	101.716136	4234	22.4029	0.217394	1385 ± 29	0.892 ± 0.019	**17864 ± 1715**
Downstream from fault								
SLH-6	30.24065	101.716334	4231	23.0636	0.225397	1446 ± 29	0.939 ± 0.019	**18766 ± 1797**
SLH-7	30.239196	101.715253	4229	21.9617	0.233501	1512 ± 29	1.068 ± 0.021	**21209 ± 2021**
SLH-8	30.239021	101.714604	4223	23.1584	0.220267	1782 ± 33	1.127 ± 0.021	**22346 ± 2125**
SLH-9	30.238639	101.713716	4224	21.5421	0.240683	1378 ± 31	1.023 ± 0.023	**20337 ± 1941**
SLH-10	30.238536	101.712427	4224	20.5288	0.217702	1952 ± 37	1.377 ± 0.027	**26766 ± 2572**
Yangjiagou site								
Upstream from fault								
YJG-1	30.051155	101.928773	3502	21.6218	0.231963	846 ± 35	0.601 ± 0.025	**17652 ± 1749**
YJG-2	30.050693	101.928255	3514	23.8309	0.221088	541 ± 23	0.330 ± 0.014	**9834 ± 963**
YJG-3	30.05033	101.928019	3521	23.4947	0.238118	525 ± 20	0.350 ± 0.013	**10386 ± 1011**
YJG-4	30.049068	101.926476	3562	23.4815	0.220780	595 ± 26	0.369 ± 0.016	**10708 ± 1154**
Downstream from fault								
YJG-5	30.053471	101.929568	3475	21.8600	0.224268	911 ± 33	0.619 ± 0.023	**18391 ± 1817**
YJG-6	30.053703	101.929608	3477	23.6030	0.220677	472 ± 20	0.290 ± 0.013	**8779 ± 871**
YJG-7	30.054779	101.929665	3475	23.6888	0.230937	557 ± 15	0.358 ± 0.010	**10887 ± 1058**
YJG-8	30.056091	101.930036	3458	24.1258	0.234527	410 ± 12	0.261 ± 0.008	**7954 ± 779**
YJG-9	30.054313	101.929677	3475	23.9211	0.224678	869 ± 21	0.540 ± 0.014	**16217 ± 1542**

Samples were processed at the Institute of Crustal Dynamics, China Earthquake Administration, Beijing; and the ^{10}Be/^{9}Be ratios were measured at GNS Science in New Zealand.
Ages are calculated with the CRONUS 2.3 calculator. LS dep = Lal (1991)/Stone (2000) time-dependent production rate model.
All samples are granite (density is 2.7 g/cm^3) except those with * which are quartzite (density is 2.65 g/cm^3); Shielding factor is 0.98. Thickness is ~5 cm. No erosion rate was applied. Standards used at GNS are '01-5-3' and '01-5-4' with ^{10}Be isotope ratios of 6.32×10–12 and 2.85×10–12, respectively, equivalent to 07KNSTD.
[a] External uncertainties (analytical and production rate, Balco et al., 2008) are reported at the 1 σ confidence level.

the YJG moraine somewhat unique. The <2 km-long eastern lateral moraine is well-preserved and covered by small bushes and medium-sized granite boulders (up to 5 m of diameter) (Fig. 4E), while only a small remnant of the western crest is preserved most likely due to rockslides along the very steep slopes above (Fig. 4C).

We collected nine samples on the YJG moraine crests from the top of large embedded granite boulders. Four samples were collected upstream from the fault (YJG-1-4) and five downstream (YJG-5-9) (Figs. 4C and S9). The ages range from 8 ± 1 ka to 18 ± 2 ka. The ages cluster in two groups from 8 ± 1 to 11 ± 1 ka and from 16 ± 2 to 18 ± 2 ka (Fig. 4D and Table 1). However, since no anomalously old sample is present, the oldest age of the moraine is taken to best represent the moraine's abandonment age and, as at SLH, also corresponds to the LGM (~20 ka). Measuring the offset in the field using a tape allowed us to determine the horizontal offset of 80 ± 5 m (Figs. 4E and S10), with no clear vertical offset. Matching the 80 ± 5 m offset with the 18 ± 2 ka age yields a late Quaternary horizontal slip rate of 4.4 ± 0.5 mm/yr.

7. Discussion

7.1. Selaha fault slip rate at various time scales

Along the clearest section of the Selaha fault, we quantitatively determined late Quaternary horizontal slip rates of 5.7–9.9 mm/yr at the TG site ('TG' in Fig. 5) and 8.1–12 mm/yr at the SLH site ('SLH1 and SLH2' in Fig. 5). However, favoring SLH1 as explained above yields a rate of 9.6–12 mm/yr. Therefore, a conservative estimate of the left-lateral rate on that part of the Selaha fault ranges between 5.7 and 12 mm/yr since ~20 ka (light gray zone in Fig. 5). Assuming that the rate should be the same at the two TG and SLH sites would narrow the rate down to between 9.6 and 9.9 mm/yr (dark gray zone in Fig. 5). The conservative rates we determined along the Selaha fault are on the same order as the rates qualitatively obtained along the same fault by Allen et al. (1991) and Chen et al. (2016), ~7.2 and 6.7 ± 3 mm/yr (near the TG and SLH sites), respectively (Table 2 and #16 and 17 in Fig. 5). The overlap rate between 9.6 and 9.9 mm/yr is also compatible with these previous estimates, but much more precise, and is the rate we will consider in the following discussion.

At the YJG site, we quantitatively determined a late Quaternary horizontal slip rate of 3.9–4.9 mm/yr ('YJG' in Fig. 5) that is significantly smaller than at the two other sites. This is most probably due to the fact that the parallel, active Zheduotang fault shares slip rate with the Selaha fault at this longitude. Taking a slip rate for the Selaha fault between 9.6 and 9.9 mm/yr and assuming that the Yalahe fault is currently inactive, the 4.4 mm/yr rate at YJG suggests that the Zheduotang fault may slip at ~5 mm/yr.

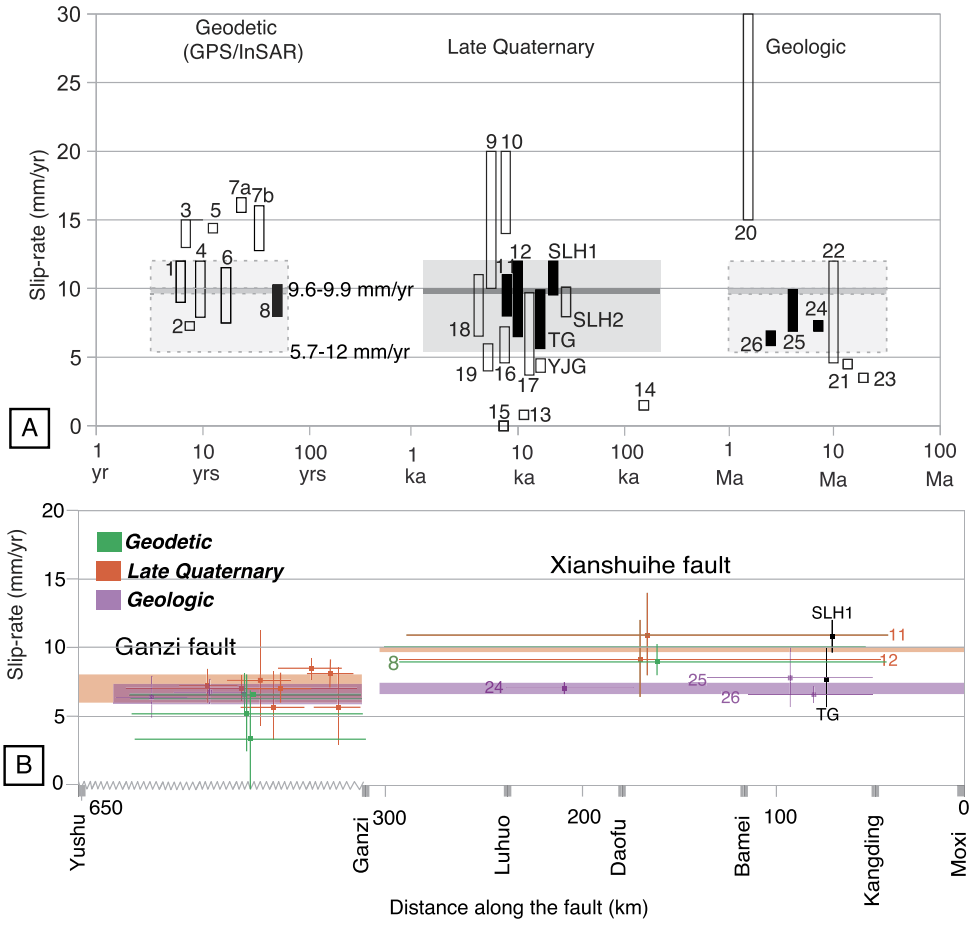

Fig. 5. Summary of left-lateral slip rates along the Xianshuihe and Ganzi faults at various time scales. See Table 2 for references to numbers. (A) Left-lateral slip rates along the XSH fault at various time scales. Open symbols represent rates that we think are not well constrained or do not correspond to the full-rate (see text for details). Plain symbols represent studies that appear better constrained. These latter rates are in agreement with our conservative rate (light gray shaded area) and close to, while sometimes lower than, the more precise rate deduced from the TG and SLH sites (dark gray shaded area). See text for details. (B) Variation of strike-slip rates along strike of the Ganzi and Xianshuihe faults at different time scales (represented by various colors). Same numbers as in A for the XSH fault. Values for the Ganzi fault can be found in Chevalier et al. (2017). Light orange and purple shaded areas respectively represent the best constrained late Quaternary and geologic rates (this study; Chevalier et al., 2017). (For interpretation of the references to color in this figure legend, the reader is referred to the web version of this article.)

At the geological time scale (several Ma), a wide range of slip rates on the XSH fault has been proposed: between 3.5 and 30 mm/yr (#20–23 in Fig. 5). All these rates have been calculated considering the same total offset (~60 km) but with very different timing of initiation of the fault (from 2 to 17 Ma). From thermochronological data, Zhang et al. (2017) determined that the Yalahe segment of the fault initiated at 8.6 ± 0.5 Ma and that motion switched to the Selaha/Zheduotang segments at 4 ± 0.4 Ma, yielding an average slip rate of 7.2 ± 0.4 mm/yr along the XSH fault (#24 in Fig. 5). Using Zhang et al. (2017)'s data yields 8.4 ± 1.6 mm/yr (62 km minus BB' and CC' = 37 km offset between 8.6 ± 0.5 and 4 ± 0.4 Ma – #25 in Fig. 5) along the Yalahe fault and 6.3 ± 0.6 mm/yr (BB'+CC' = 25 km offset since 4 ± 0.4 Ma – #26 in Fig. 5) along the Selaha/Zheduotang faults. The geologic slip rates are in the range of the conservative slip rate (5.7–12 mm/yr) but are 20–30% lower than the more precise rate we determined for the Selaha fault at the 20 ka time scale (9.6–9.9 mm/yr).

Slip rates on the XSH fault have been estimated at a much shorter time scale (a few years) by GPS (both from profiles across the fault and from block models) and InSAR data. One important question is whether these data reflect the interseismic rate of the fault. Such rates vary between 7 and 16.7 mm/yr (Table 2 and #1 to 8 in Fig. 5). Among these results, Jiang et al. (2015b) have built a 3D viscoelastic model from the joint inversion of GPS and InSAR data. Depending on the viscosity assumed for the lower crust, between 10^{18} to 10^{21} Pa.s, the satisfying models yield slip rates ranging from 7 to 14.7 mm/yr on 6 segments along the XSH fault, that globally decrease from NW to SE (Jiang et al., 2015b). The rate along segment S5 (Selaha) in Jiang et al. (2015b), along which our SLH and TG sites are located, ranges from 7 to 7.4 mm/yr (#2 in Fig. 5), which is significantly lower than the rate we determined. From a single GPS dataset, Y. Wang et al. (2017) deduce two different slip rates whether considering profiles across the fault (15.5–16.7 mm/yr, #7a in Fig. 5) or a block model (12.3–15.9 mm/yr, #7b in Fig. 5). Zheng et al. (2017) measured a rate of 9.1 ± 1 mm/yr along a profile across the fault based on the most complete picture of interseismic velocities available to date (#8 in Fig. 5). Out of these nine estimates, four are significantly faster than the late Quaternary rate we determined, including many estimates made with recent dataset built on a 1999 to 2014 period (#3, #7a, #7b in Fig. 5; Y. Wang et al., 2017; W. Wang et al., 2017). These estimates certainly have limitations (for instance, the block model proposed by W. Wang et al., 2017, produces systematic pluri-millimetric residuals in the vicinity of the Selaha segment) but they overall remain reasonable. The one estimate that is significantly lower than the late Quaternary estimate comes from the only viscoelastic modeling of the Xianshuihe fault system including detailed inversion of interseismic coupling on the fault (Jiang et al., 2015b, #2 in Fig. 5). Interestingly, the most recent slip rate estimate to date based on the

Table 2
Slip rate summary along the Xianshuihe fault.

Segment	Slip-rate (mm/yr)	Reference	Method	Ref. in Fig. 5
XSH fault	9–12	Wang et al. (2009)	InSAR near Luhuo	1
	7–7.4	Jiang et al. (2015b)	Visco-elastic model with InSAR and GPS Data	2
	13–15	W. Wang et al. (2017)	GPS – block model	3
	8–12	Shen et al. (2005)	GPS – rigid blocks	4
	14.4	Gan et al. (2007)	GPS – dislocation	5
	7.5–11.5	Zhang (2013)	GPS – profiles	6
	15.5–16.7	Y. Wang et al. (2017)	GPS – profiles	7a
	12.3–15.9	Y. Wang et al. (2017)	GPS – block model	7b
	8–10.2	Zheng et al. (2017)	GPS – profiles	8
XSH fault	10–20	Allen et al. (1991)	inferred ages	9
	14–20	Chen et al. (2008)	lower terrace age	10
	8–11	Zhang (2013)	reinterpretation of Chen et al. (2008), using upper terrace age	11
	6.5–12	Chevalier et al. (2017)	using their MGT ages along the Ganzi fault	12
Yalahe fault	0.8	Allen et al. (1991)	inferred ages	13
	1.5	Chen et al. (2016)	one thermoluminescence age	14
	0	**This study**	field work	15
Selaha fault	4.6–7.2	Allen et al. (1991)	inferred ages	16
	3.7–9.7	Chen et al. (2016)	geomorphic correlations	17
	7.6(+2.3/−1.9)	**This study, TG site**	^{10}Be	TG
	10.7(+1.3/−1.1)	**This study, SLH site**	^{10}Be	SLH1
	9(+1.1/−0.9)	**This study, SLH site**	^{10}Be	SLH2
	3.9–4.9	**This study, YJG site**	^{10}Be	YJG
Zheduotang fault	6.5–10.5	Chen et al. (2016)	one ^{14}C, one OSL ages	18
	4–6	Zhang et al. (2016)	^{14}C	19
XSH fault	15–30	Wang et al. (1998)	62 km in 2–4 Ma	20
	∼4.5	Roger et al. (1995)	62 km in 13 Ma	21
	4.6–12	Yan and Lin (2015)	62 km in 5–13 Ma	22
	∼3.5	Wang et al. (2012)	62 km in 17 ± 2 Ma	23
	6.8–7.6	Zhang et al. (2017)	62 km since 8.6 ± 0.5 Ma	24
Yalahe fault	6.8–10	Zhang et al. (2017)	37 km between 8.6 ± 0.5 Ma and 4 ± 0.4 Ma	25
Selaha/Zheduotang	5.7–6.9	Zhang et al. (2017)	25 km since 4 ± 0.4 Ma	26

longest GPS record published so far by Zheng et al. (2017) is 8 to 10.2 mm/yr, i.e., consistent with our findings. It is nonetheless possible that only four rates (#1, #4, #6, #8 in Fig. 5) effectively capture the long-term rate along the fault, but no clear technical nor scientific bias allows to reject the other estimates that could also reflect changes in the rate along the XSH fault in the last few years. This relatively high variability in geodetic rate estimates emphasizes that caution is needed when using geodetic data to discuss the precise present-day rate and the seismic risk of a continental strike-slip fault such as the Xianshuihe fault system. Despite the significant instrumental effort made in recent years in the area, too few robust velocity measurements remain available due to too short time-lapse measurements and due to the lack of small-scale denser networks specifically designed to assess individual fault rates. In such cases, it would be wise to wait several more years before reaching geodynamic conclusions as suggested by Zhao et al. (2015). Despite their variability, short-term studies share common features, in particular, most of them imply an increase of the slip rate from the Ganzi fault to the XSH fault.

7.2. Slip rate comparison at various time scales between different fault segments of the Xianshuihe fault system

NW of the XSH fault, the slip rate along the Ganzi fault (∼300 km) is spatially constant at 6–8 mm/yr at the late Quaternary time scale (Chevalier et al., 2017) (Fig. 5B), determined using similar methods as in this paper. This rate is consistent with geologic slip rates of 4.9–7.5 mm/yr, obtained by matching the Queer Shan pluton and Jinsha River offsets with the fault's initiation age (12.6 ± 1 Ma), and is somewhat compatible with geodetic rates using the most recent GPS studies (<8 mm/yr) or InSAR (6.4 mm/yr) (left part of Fig. 5B, see Chevalier et al., 2017 and references therein for a review).

Along the XSH fault, our 9.6–9.9 mm/yr late Quaternary slip rate is higher than the slip rate along the Ganzi fault (Fig. 5B). Similarly, most short-term studies imply a southeastward increase of the strike-slip rate between the Ganzi and XSH fault segments (Zhang, 2013; W. Wang et al., 2017; Y. Wang et al., 2017) (Fig. 5B). This trend is much less clear for geologic rates that could be considered as similar all along the Ganzi and the XSH faults at 7 ± 1 mm/yr since ∼9 Ma (Fig. 5B). This suggests that since the onset of the XSH fault, its slip rate has increased to finally reach its present day value. In order for the present day slip rate to increase from ∼7 to ∼9.75 mm/yr (9.6–9.9 mm/yr) and for the average rate to be ∼7.2 mm/yr, the rate increase has to be quite recent, i.e. less than ∼1 Ma ago.

Considering that the whole Xianshuihe fault system is a transform fault would yield a rotation pole located at 25.082942°N/93.574735°E, close to the eastern Himalayan syntaxis (Fig. 6). This strongly suggests that the left-lateral motion along the Xianshuihe fault system is directly linked to the collision of India within Asia. It has long been noted that the shape of the fault system closely follows that of a potential slip line in a plastic medium indented by a rigid medium with a corner shape (inset in Fig. 6) (Tapponnier and Molnar, 1976). However such conceptual framework does not explain why the strike-slip rate would be lower on the Ganzi fault than on the XSH fault. A first interpretation could be that the Ganzi fault is located closer to the pole (∼8.4°) than the XSH fault (∼8.8°), and thus that the corresponding rate is smaller (Fig. 6). However such a small difference in angular distance would only explain a small fraction (∼0.4 mm/yr or less than a quarter) of the rate increase between the Ganzi and XSH faults (∼2 mm/yr).

The above hypothesis was assuming that the Xianshuihe fault system is separating only two blocks. However the northern block corresponds in fact to several blocks. First the Longmenshan reverse/dextral fault zone separates the Sichuan and the Longmenshan blocks (Fig. 6). Second, it has recently been suggested that, even if the active Longriba reverse/dextral fault system is discontinuous in the morphology, it nevertheless appears to be a significant boundary between the Longmenshan and Bayan Har

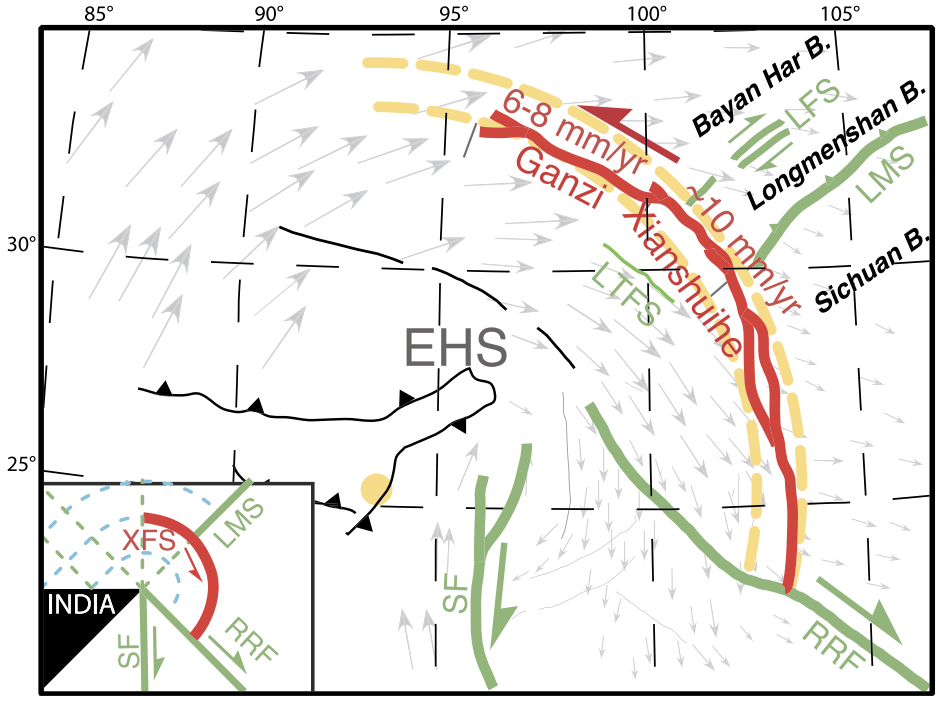

Fig. 6. Conceptual 2D model of the eastern corner of the India–Asia collision. Slip rates determined by Chevalier et al. (2017) along the Ganzi fault and this study along the XSH fault are shown. LFS = Longriba fault system, LTFS = Litang fault system, LMS = Longmenshan, XFS = Xianshuihe fault system, XSH = Xianshuihe, RRF = Red River fault, SF = Sagaing fault. Orange dashed line shows how well a small circle whose pole of rotation (orange circle, 25.082942°N–93.574735°E) is located in the eastern Himalayan syntaxis (EHS) fits the trace of the XFS. Grey arrows show GPS vectors relative to stable Eurasia (W. Wang et al., 2017). Inset shows the conceptual 2D model where a rigid indenter (India) enters Asia (modified from Tapponnier and Molnar, 1976). (For interpretation of the references to color in this figure legend, the reader is referred to the web version of this article.)

blocks (Xu et al., 2008; Guo et al., 2015; Ren et al., 2013a, 2013b; Ansberque et al., 2015, 2016) (Fig. 6). A study of the Longriqu fault, NW segment of the Longriba fault system suggests a Holocene right-lateral rate of $\leq 3.2 \pm 1.1$ mm/yr since 13 ka (Ansberque et al., 2016). Most GPS datasets document a change in the rate of motion with respect to stable Eurasia across the Longriba fault system (Fig. 6) (e.g., Gan et al., 2007; W. Wang et al., 2017; Y. Wang et al., 2017). The corresponding block models distinguish the Bayan Har block to the west, moving faster, and the Longmenshan block to the east of the fault, moving slower. This corresponds to a lower left-lateral relative motion across the Ganzi fault than across the XSH fault to the east of the intersection with the Longriba fault system (Fig. 6). Nevertheless, as stated above, the geologic rates could be considered as similar all along the Ganzi and XSH faults at 7 ± 1 mm/yr (Fig. 5B). These data thus suggest that the rate increase along the XSH fault results from the onset of the present-day kinematics of the Longriba fault system that would thus be less than ~1 Ma old.

7.3. Earthquake hazard along the Xianshuihe fault

The discontinuous and geometrically complicated Selaha fault (~60 km long) is the clearest in the topography of the SE XSH fault, with a horizontal slip rate higher than that along the Yalahe or Zheduotang segments, showing that it is the main fault connecting the XSH fault NW of Bamei to the Moxi fault SE of Kangding. It also most likely implies that large earthquakes repeatedly happen on the Selaha fault, as it regularly did along the entire XSH fault in the past (green stars in Fig. 1B). Because the 2014 Kangding earthquakes have not released all the energy accumulated since the 1955 Kangding earthquake that occurred on the same fault (Jiang et al., 2015a), extra measures should be taken to prevent more damage to Kangding (population ~150000) due to an upcoming large earthquake, as suggested by studies following the 2008 Wenchuan earthquake.

Assuming that the entire Selaha–Kangding segment of the XSH fault (~60 km long) is entirely locked from surface to 15 km depth, and accommodates between 5.7 and 12 mm/yr of strike-slip motion, the current moment accumulation rate on the fault would be 1.54–3.24 × 10E17 Nm/yr (the rigidity $\mu = 30$ GPa). Assuming that this moment accumulation rate is constant since the 1955 Mw7 Kangding earthquake, the Selaha-Kangding segment has accumulated between 9.54E18 and 2E19 Nm. Because the 2014 seismic sequence only released ~1.18E18 Nm (Jiang et al., 2015a), the remaining potential for moment release over this segment is still high and could afford for a 6.5 to 6.8 earthquake.

8. Conclusion

The 1400 km-long Xianshuihe fault system is one of the most active fault system in China and almost its entire length has rupture since 1700. The last large earthquake occurred in 2014 near Kangding (Kangding earthquakes, Mw5.9 and Mw5.6) along the Selaha segment of the SE XSH fault. This section of the Xianshuihe fault system had been interpreted by many authors to correspond to a seismic gap and to be highly at risk, especially following the 2008 Wenchuan and 2013 Lushan earthquakes.

We studied three sites (offset moraines and levees) located along the Selaha fault to determine its late Quaternary slip rate and assess its seismic hazard. We determined horizontal slip rates of ~10 mm/yr at Tagong (TG) and Selaha (SLH) sites where the fault is single-stranded. A rate of 3.9–4.9 mm/yr is found at the Yangjiagou (YJG) site, where the fault is parallel to the Zheduotang fault, therefore suggesting a rate of ~5 mm/yr along the latter.

The late Quaternary slip rate we determined along the SE XSH fault is higher than that along the Ganzi fault to the NW (6–8 mm/yr). This appears to be linked to the existence of the Longriba fault system that separates the Longmenshan and Bayan Har blocks north of the Xianshuihe fault system.

A higher slip rate along the short (~60 km) and discontinuous Selaha fault compared to that along the long (~300 km) and linear Ganzi fault suggests a high earthquake hazard in the Kangding area in the near future, with an earthquake of $M > 6$, which could devastate the densely populated city of Kangding.

Acknowledgements

This project was conducted under the auspices of the Natural National Science Foundation of China [NSFC 41672210, 41672211], the China Geological Survey [project DD20160022], the Basic Outlay of Scientific Research Work from the Institute of Geology, CAGS [J1528]. We thank Shiguang Wang for his help in the field.

Appendix A. Supplementary material

Supplementary material related to this article can be found online at https://doi.org/10.1016/j.epsl.2017.12.045.

References

Allen, C.R., Luo, Z., Qian, H., Wen, X., Zhou, H., Huang, W., 1991. Field study of a highly active fault zone: the XSF of southwestern China. Geol. Soc. Am. Bull. 103, 1178–1199.

Ansberque, C., Godard, V., Bellier, O., De Sigoyer, J., Liu-Zeng, J., Xu, X., Ren, Z., Li, Y., A.S.T.E.R. Team, 2015. Denudation pattern across the Longriba fault system and implications for the geomorphological evolution of the eastern Tibetan margin. Geomorphology 246, 542–557. https://doi.org/10.1016/j.geomorph.2015.07.017.

Ansberque, C., Bellier, O., Godard, V., Lasserre, C., Wang, M., Braucher, R., Talon, B., de Sigoyer, J., Xu, X., Bourles, D., 2016. The Longriqu fault zone, eastern Tibetan Plateau: segmentation and Holocene behavior. Tectonics 35. https://doi.org/10.1002/2015TC004070.

Balco, G., Stone, J.O., Lifton, N.A., Dunai, T.J., 2008. A complete and easily accessible means of calculating surface exposure ages or erosion rates from ^{10}Be and ^{26}Al measurements. Quat. Geochronol. 3, 174–195. https://doi.org/10.1016/j.quageo.2007.12.001.

Chen, G., Xu, X., Wen, X., Wang, Y., 2008. Kinematical transformation and slip partitioning of northern to eastern active boundary belt of Sichuan–Yunnan block. Seismol. Geol. 30, 58–85 (in Chinese).

Chen, G., Xu, X., Wen, X., Chen, Y., 2016. Late Quaternary slip-rates and slip-partitioning on the southeastern Xianshuihe fault system, eastern Tibetan Plateau. Acta Geol. Sin. 90, 537–554.

Chevalier, M.-L., Hilley, G., Tapponnier, P., Van Der Woerd, J., Liu-Zeng, J., Finkel, R.C., Ryerson, F.J., Li, H., Liu, X., 2011. Constraints on the late Quaternary glaciations in Tibet from cosmogenic exposure ages of moraine surfaces. Quat. Sci. Rev. 30, 528–554. https://doi.org/10.1016/j.quascirev.2010.11.005.

Chevalier, M.L., Leloup, P.H., Replumaz, A., Pan, J., Metois, M., Li, H., 2017. Temporally constant slip-rate along the Ganzi fault, NW Xianshuihe fault system, eastern Tibet. Geol. Soc. Am. Bull. https://doi.org/10.1130/B31691.1. In press.

Cowgill, E., 2007. Impact of riser reconstructions on estimation of secular variation in rates of strike-slip faulting: revisiting the Cherchen River site along the Altyn Tagh fault, NW China. Earth Planet. Sci. Lett. 254 (3–4), 239–255. https://doi.org/10.1016/j.epsl.2006.09.015.

Fu, P., Stroeven, A.P., Harbor, J.M., Hattestrand, C., Heyman, J., Caffee, M.W., Zhou, L., 2013. Paleoglaciation of Shaluli Shan, southeastern Tibetan Plateau. Quat. Sci. Rev. 64, 121–135. https://doi.org/10.1016/j.quascirev.2012.12.009.

Gan, W., Zhang, P., Shen, Z., Niu, Z., Wang, M., Wan, Y., Zhou, D., Cheng, J., 2007. Present-day crustal motion within the Tibetan Plateau inferred from GPS measurements. J. Geophys. Res. 112, B08416. https://doi.org/10.1029/2005JB004120.

Gaudemer, Y., Tapponnier, P., Turcotte, D.L., 1989. River offsets across active strike-slip faults. Ann. Tecton. 3 (2), 55–76.

Guo, X., Gao, R., Keller, G.R., Yin, A., Xiong, X., 2015. Longriba fault zone in eastern Tibet: an important tectonic boundary marking the westernmost edge of the Yangtze block. Tectonics 34. https://doi.org/10.1002/2015TC003880.

Hallet, B., Putkonen, J., 1994. Surface dating of dynamic landforms: young boulders on aging moraines. Science 265, 937–940.

Heyman, J., Stroeven, A.P., Harbor, J., Caffee, M.W., 2011. Too young or too old: evaluating cosmogenic exposure dating based on an analysis of compiled boulder exposure ages. Earth Planet. Sci. Lett. 302, 71–80. https://doi.org/10.1016/j.epsl.2010.11.040.

Jiang, G., Wen, Y., Liu, Y., Xu, X., Fang, L., Chen, G., Meng, G., Xu, C., 2015a. Joint analysis of the 2014 Kangding, southwest China, earthquake sequence with seismicity relocation and InSAR inversion. Geophys. Res. Lett. https://doi.org/10.1002/2015GL063750.

Jiang, G., Xu, X., Chen, G., Liu, Y., Fukahata, Y., Wang, H., Yu, G., Tan, X., Xu, C., 2015b. Geodetic imaging of potential seismogenic asperities on the Xianshuihe–Anninghe–Zemuhe fault system, southwest China, with a new 3-D viscoelastic interseismic coupling model. J. Geophys. Res. Lett. https://doi.org/10.1002/2014JB011492.

Lal, D., 1991. Cosmic-ray labeling of erosion surfaces: in situ nuclide production rates and erosion models. Earth Planet. Sci. Lett. 104 (2–4), 424–439. https://doi.org/10.1016/0012-821X(91)90220-C.

Liang, S., Gan, W., Shen, C., Xiao, G., Liu, J., Chen, W., Ding, X., Zhou, D., 2013. Three-dimensional velocity field of present-day crustal motion of the Tibetan Plateau derived from GPS measurements. J. Geophys. Res. 118 (10), 2013JB010503.

Ou, X., Lai, Z., Zhou, S., Zeng, L., 2014. Timing of glacier fluctuations and trigger mechanisms in eastern Qinghai–Tibetan Plateau during the late Quaternary. Quat. Res. 81, 464–475. https://doi.org/10.1016/j.yqres.2013.09.007.

Parsons, T., Ji, C., Kirby, E., 2008. Stress changes from the 2008 Wenchuan earthquake and increased hazard in the Sichuan basin. Nature. https://doi.org/10.1038/nature07177.

Putkonen, J., Swanson, T., 2003. Accuracy of cosmogenic ages for moraines. Quat. Res. 59, 255–261. https://doi.org/10.1016/S0033-5894(03)00006-1.

Ren, J., Xu, X., Yeats, R.S., Zhang, S., Ding, R., Gong, Z., 2013a. Holocene paleoearthquakes of the Maoergai fault, eastern Tibet. Tectonophysics 590, 121–135. https://doi.org/10.1016/j.tecto.2013.01.017.

Ren, J., Xu, X., Yeats, R.S., Zhang, S., 2013b. Latest Quaternary paleoseismology and slip rates of the Longriba fault zone, eastern Tibet: implications for fault behavior and strain partitioning. Tectonics 32, 1–23. https://doi.org/10.1002/tect.20029.

Roger, F., Calassou, S., Lancelot, J., Malavieille, J., Mattauer, M., Xu, Z., Hao, Z., Hou, L., 1995. Miocene emplacement and deformation of the Konga Shan granite (Xianshui He fault zone, west Sichuan, China): geodynamic implications. Earth Planet. Sci. Lett. 130, 201–216.

Schafer, J.M., Tschudi, S., Zhao, Z., Wu, X., Ivy-Ochs, S., Wieler, R., Baur, H., Kubik, P.W., Schluchter, C., 2002. The limited influence of glaciations in Tibet on global climate over the past 170000 yr. Earth Planet. Sci. Lett. 194, 287–297.

Shao, Z., Xu, J., Ma, H., Zhang, L., 2016. Coulomb stress evolution over the past 200 years and seismic hazard along the Xianshuihe fault zone of Sichuan, China. Tectonophysics 670, 48–65. https://doi.org/10.1016/j.tecto.2015.12.018.

Shan, B., Xiong, X., Zheng, Y., Jin, B., Liu, C., Xie, Z., Hsu, H., 2013. Stress changes on major faults caused by 2013 Lushan earthquake and its relationship with 2008 Wenchuan earthquake. Sci. China Earth Sci. 56, 1169–1176. https://doi.org/10.1007/s11430-013-4642-1.

Shen, Z., Lu, J., Wang, M., Burgmann, R., 2005. Contemporary crustal deformation around the southeast borderland of the Tibetan Plateau. J. Geophys. Res. 110, B11409. https://doi.org/10.1029/2004JB003421.

Stone, J.O., 2000. Air pressure and cosmogenic isotope production. J. Geophys. Res. 105, 23753–23759. https://doi.org/10.1029/2000JB900181.

Strasky, S., Graf, A.A., Zhao, Z.Z., Kubik, P.W., Baur, H., Schluchter, C., Wieler, R., 2009. Late Glacial ice advances in southeast Tibet. J. Asian Earth Sci. 34, 458–465.

Tapponnier, P., Molnar, P., 1976. Slip-line field theory and large-scale continental tectonics. Nature 264 (5584), 319–324. https://doi.org/10.1038/264319a0.

Toda, S., Lin, J., Meghraoui, M., Stein, R.S., 2008. 12 May 2008 M = 7.9 Wenchuan, China, earthquake calculated to increase failure stress and seismicity rate on three major fault systems. Geophys. Res. Lett. 35, L17305. https://doi.org/10.1029/2008GL034903.

Wang, E., Burchfiel, B.C., Royden, L.H., Chen, L., Chen, J., Li, W., Chen, Z., 1998. The Cenozoic Xianshuihe–Xiaojiang, Red River, and Dali Fault Systems of southwestern Sichuan and central Yunnan, China. Spec. Pap., Geol. Soc. Am., vol. 327. 108 p.

Wang, E., Burchfiel, B.C., 2000. Late Cenozoic to Holocene deformation in southwestern Sichuan and adjacent Yunnan, China, and its role in formation of the southeastern part of the Tibetan Plateau. Geol. Soc. Am. Bull. 112, 413–423.

Wang, H., Wright, T.J., Biggs, J., 2009. Interseismic slip rate of the northwestern Xianshuihe fault from InSAR data. Geophys. Res. Lett. 36, L03302. https://doi.org/10.1029/2008GL036560.

Wang, S., Jiang, G., Xu, T., Tian, Y., Zheng, D., Fang, X., 2012. The Jinhe–Qinghe fault—an inactive branch of the Xianshuihe–Xiaojiang fault zone, eastern Tibet. Tectonophysics 544–545, 93–102. https://doi.org/10.1016/j.tecto.2012.04.004.

Wang, W., Qiao, X., Yang, S., Wang, D., 2017. Present-day velocity field and block kinematics of Tibetan Plateau from GPS measurements. Geophys. J. Int. 208, 1088–1102. https://doi.org/10.1093/gji/ggw445.

Wang, Y., Wang, M., Shen, Z., 2017. Block-like versus distributed crustal deformation around the northeastern Tibetan plateau. J. Asian Earth Sci. 140, 31–47. https://doi.org/10.1016/j.jseaes.2017.02.040.

Wen, X., 2000. Character of rupture segment of Xianshuihe–Zemuhe–Anninghe fault zone, western Sichuan. Seismol. Geol. 22, 239–249.

Wen, X.Z., Ma, S.L., Xu, X.W., He, Y.N., 2008. Historical pattern and behavior of earthquake ruptures along the eastern boundary of the Sichuan–Yunnan faulted-block, southwestern China. Phys. Earth Planet. Inter. 168 (1–2), 16–36. https://doi.org/10.1016/j.pepi.2008.04.013.

Xie, Z., Zheng, Y., Liu, C., Shan, B., Riaz, M.S., Xiong, X., 2017. An integrated analysis of source parameters, seismogenic structure, and seismic hazards related to the 2014 MS 6.3 Kangding earthquake, China. Tectonophysics 712, 1–9.

Xu, X., Wen, X., Chen, G., Yu, G., 2008. Discovery of the Longriba fault zone in eastern Bayan Har block, China and its tectonic implication. Sci. China Ser. D 51 (9), 1209–1223. https://doi.org/10.1007/s11430-008-0097-1.

Xu, L.B., Zhou, S.Z., 2009. Quaternary glaciations recorded by glacial and fluvial landforms in the Shaluli Mountains, southeastern Tibetan Plateau. Geomorphology 103, 268–275. https://doi.org/10.1016/j.geomorph.2008.04.015.

Xu, L.B., Ou, X.J., Lai, Z.P., Zhou, S.Z., Wang, J., Fu, Y.C., 2010. Timing and style of late Pleistocene glaciation in the Queer Shan, northern Hengduan Mountains in the eastern Tibetan Plateau. J. Quat. Sci. 25, 957–966. https://doi.org/10.1002/jqs.1379.

Yan, B., Lin, A., 2015. Systematic deflection and offset of the Yangtze River drainage system along the strike-slip Ganzi–Yushu–Xianshuihe fault zone, Tibetan Plateau. J. Geodyn. 87, 13–25. https://doi.org/10.1016/j.jog.2015.03.002.

Yang, W., Cheng, J., Liu, J., Zhang, X., 2015. The Kangding earthquake swarm of November, 2014. Earthq. Sci. 28 (3), 197–207. https://doi.org/10.1007/s11589-015-0123-2.

Zechar, J.D., Frankel, K.L., 2009. Incorporating and reporting uncertainties in fault slip rates. J. Geophys. Res. 114, B12407. https://doi.org/10.1029/2009JB006325.

Zhang, B., Ou, X.J., Lai, Z.P., 2012. OSL ages revealing the glacier retreat in the Dangzi valley in the eastern Tibetan Plateau during the Last Glacial Maximum. Quat. Geochronol. 10, 244–249. https://doi.org/10.1016/j.quageo.2012.01.013.

Zhang, P.Z., 2013. A review on active tectonics and deep crustal processes of the western Sichuan region, eastern margin of the Tibetan Plateau. Tectonophysics 584, 7–22. https://doi.org/10.1016/j.tecto.2012.02.021.

Zhang, Y., Yao, X., Yu, K., Du, G., Guo, C., 2016. Late Quaternary slip-rate and seismic activity of the Xianshuihe fault zone in southwest China. Acta Geol. Sin. 90, 525–536.

Zhang, Y., Replumaz, A., Leloup, P.H., Wang, G., Bernet, M., van der Beek, P., Paquette, J.L., Chevalier, M.L., 2017. Cooling history of the Gongga batholith: implications for the Xianshuihe fault and Miocene kinematics of SE Tibet. Earth Planet. Sci. Lett. 465, 1–15. https://doi.org/10.1016/j.epsl.2017.02.025.

Zhao, B., Huang, Y., Zhang, C., Wang, W., Tan, K., Du, R., 2015. Crustal deformation on the Chinese mainland during 1998–2014 based on GPS data. Geodesy Geodyn. 6, 7–15. https://doi.org/10.1016/j.geog.2014.12.006.

Zheng, G., Wang, H., Wright, Tim J., Lou, Y., Zhang, R., Zhang, W., Shi, C., Huang, J., Wei, N., 2017. Crustal deformation in the India–Eurasia collision Zong from 25 years of GPS measurements. https://doi.org/10.1002/j.JGR.2017.09.021.